A 408-MHz radio survey of the region surrounding Simeis 57

Higgs, L.A.; Landecker, T.L.; Israel, F.P.; Bally, J.

A 408-MHz RADIO SURVEY OF THE REGION SURROUNDING SIMEIS 57

BY L.A. HIGGS AND T.L. LANDECKER
Dominion Radio Astrophysical Observatory, National Research Council, Penticton, British Columbia

F.P. ISRAEL
Sterrewacht Leiden, The Netherlands

AND

J. BALLY
AT&T Bell Laboratories, U.S.A.

(Received August 21, 1990)

ABSTRACT

In late 1985, the area surrounding the peculiar H II region Simeis 57 was observed with the DRAO Synthesis Telescope at 408 MHz. Despite the presence of Cygnus A in the field of view, which limits the sensitivity of the telescope owing to its limited dynamic range, a reasonable picture of the distribution of stronger radio sources ($S \geq 1$ Jy) in this region has been obtained. Included in the 8° field of view are the supernova remnant W 63 and the north-east portion of the Cygnus X complex of H II regions (also containing the G78.2+2.1 supernova remnant). Some 40 compact radio sources are catalogued and the extended sources are discussed. A spectral index is derived for the radio emission from Simeis 57 but it is not sufficiently precise to determine whether or not the emission is thermal. Spectral indices of many of the compact sources have been derived from the data in the literature, combined with the present results. Most sources are extragalactic, but several possible Galactic sources are identified. Two of these may be small-diameter supernova remnants.

RÉSUMÉ

A la fin de 1985, la zone entourant la curieuse région H II Simeis 57 a été observée à 408 MHz au moyen du télescope à synthèse de l'OFRA. En dépit de la présence de la source Cygnus A dans le champ de vision, ce qui limite la sensibilité du télescope du fait de sa dynamique limitée, une image de bonne qualité des sources radios les plus fortes ($S \geq 1$ Jy) de cette région a été obtenue. Le reste de la supernova W63 et la portion nord-est du complexe Cygnus X de régions H II (qui comprend aussi le reste de la supernova G78.2+2.1) se trouvaient dans le champ de 8 degrés. Quelques 40 radio sources sont cataloguées et les sources étendues sont discutées. On a déduit un indice spectral pour l'émission radio de Simeis 57 mais il n'est pas suffisamment précis pour déterminer si l'émission est thermale ou non. Les indices spectraux de beaucoup des sources compactes ont été déduits de données trouvées dans la littérature et ont été combinés aux présents résultats. La plupart des sources sont extragalactiques, mais plusieurs sources galactiques possibles sont identifiées. Deux de celles-ci pourraient être des restes de supernovae de petit diamètre.

MF

Introduction. In September 1985, two of the authors of this paper (Israel and Bally) used the aperture-synthesis radio telescope of the Dominion Radio Astrophysical Observatory (DRAO) to observe the distribution and kinematics of neutral hydrogen around the unusual H II region known as Simeis 57 (Gaze and Shajn 1951, 1955). (This object is also known as C 191 or HS 191). The results of these observations will be published elsewhere. The DRAO synthesis telescope, as well as observing the 21-cm spectral line of H I, simultaneously detects radio continuum emission at 408 MHz and 1420 MHz. In this paper, we present the results of the 408-MHz continuum observations. (The 1420-MHz continuum DRAO observations of Simeis 57 have been briefly presented, without interpretation, in a paper studying techniques for wide-field imaging using the Very Large Array (Cornwell 1988)).

Observations. The observations were made with the DRAO Synthesis Telescope, which is described in detail by Roger *et al.* (1973) and Veidt *et al.* (1985). The telescope consists of four 9-m antennas on an east-west baseline and observations were made using interferometer spacings ranging from 12.86 m to 604.29 m (in steps of 30/7 m). This yielded a resolution of about 4′ at 408 MHz. The observational parameters are listed in Table I. The observations were calibrated using the sources 3C 147 and 3C 295, using assumed flux densities consistent with the flux scale of Baars *et al.* (1977). At 408 MHz, the Synthesis Telescope has a field of view of 8°.3 diameter, defined (for this paper) by the 18% level of the primary pattern of the 9-m antennas.

The derivation of a 408-MHz map was complicated by the presence of Cygnus A, a 5000-Jy source, in the field of view. It is at the 16% level of the primary pattern, and therefore appears as a source of about 800 Jy. The inevitable small phase errors in the telescope combined with the presence of such a strong source severely limit the dynamic range of any map. The first step in the reduction was therefore an attempt to remove the contribution of Cygnus A from the observed visibilities, allowing (to the first order) for the phase and amplitude errors in the data. Smoothly varying phase and amplitude correction factors were derived that, when applied to model Cygnus A visibilities, best fitted the observed visibilities. Using these factors and the model visibilities, the contributions from Cygnus A were computed and subtracted. The resulting visibilities were then transformed to a map, which was deconvolved using the DRAO version of the CLEAN algorithm (a combination of the method of Clark (1980) and that of Steer *et al.* (1984)). The restored map was then corrected for the primary-pattern response. Since the gain of the telescope receivers is controlled by an automatic gain control (AGC) system, the map then requires a scaling correction resulting from the different system temperatures that are observed in the Simeis 57 field and for a field centred

TABLE I
PARAMETERS FOR DRAO 408-MHz OBSERVATIONS

Field centre (B1950)	$\alpha = 20^h14^m32^s$
	$\delta = +43°33'13''$
Date of observation	September 1985
Field of view (to 18%)	8.°33
Resolution (CLEAN beam)	3.′4 × 5.′0 (EW × NS)
Observed *rms* noise (field centre)	110 mJy/beam (13 K)
Calibrators and assumed flux densities	3C 147 (48 Jy), 3C 295 (54 Jy)

3C = Edge *et al.* (1959); Bennett (1962)

on a calibration source. This factor is estimated to be 1.54 ± 0.06, mainly because of the presence of Cygnus A and Cygnus X in the observed field.

Observations of fields containing a large radio flux also suffer from another instrumental effect. Truncation of the visibilities to a fixed word length can result in artefacts at the field centre. In the present case, the structure of the radio emission related to Simeis 57 (located at the field centre) was badly distorted. The effects of the truncation errors were simulated and a correction was made which makes the map look reasonable in this region. However, the detailed distribution of 408-MHz radio emission within 7′ of the field centre must be accepted with caution, and a faint negative elliptical-ring artefact, 27′ × 38′ (EW × NS) centred on the field centre, remains in the map.

The Synthesis Telescope is not sensitive to the large-scale distribution of radio emission and information on the large-scale radio structure was extracted from the 408-MHz all-sky survey of Haslam *et al.* (1982). More details on the procedure used to add the large-scale structure can be found in Joncas and Higgs (1990). In effect, single-antenna data were used for interferometer spacings less than 17 m and Synthesis Telescope data for spacings greater than 27 m, with a blend of the two in the intervening interval.

The resulting map is presented in figure 1. Clearly evident are "spoke-like" features emanating from the location of Cygnus A, which itself has been removed. These result from an unexplained modulation (in hour angle) of the Cygnus A visibilities, possibly due to periodic pointing errors in the antennas. The limitation in dynamic range that result from these and other uncorrected phase variations can be seen. The weakest sources that can be clearly detected in the map are at about the 1 Jy level, however, indicating that a dynamic range in excess of 1000 has been achieved. The map in figure 1 extends well beyond the normally-used field of view for DRAO observations in order to illustrate one particular artefact which appeared in this observation, and which will be mentioned briefly later. Normally, only the region in which the primary pattern response exceeds 20% is used, whereas in

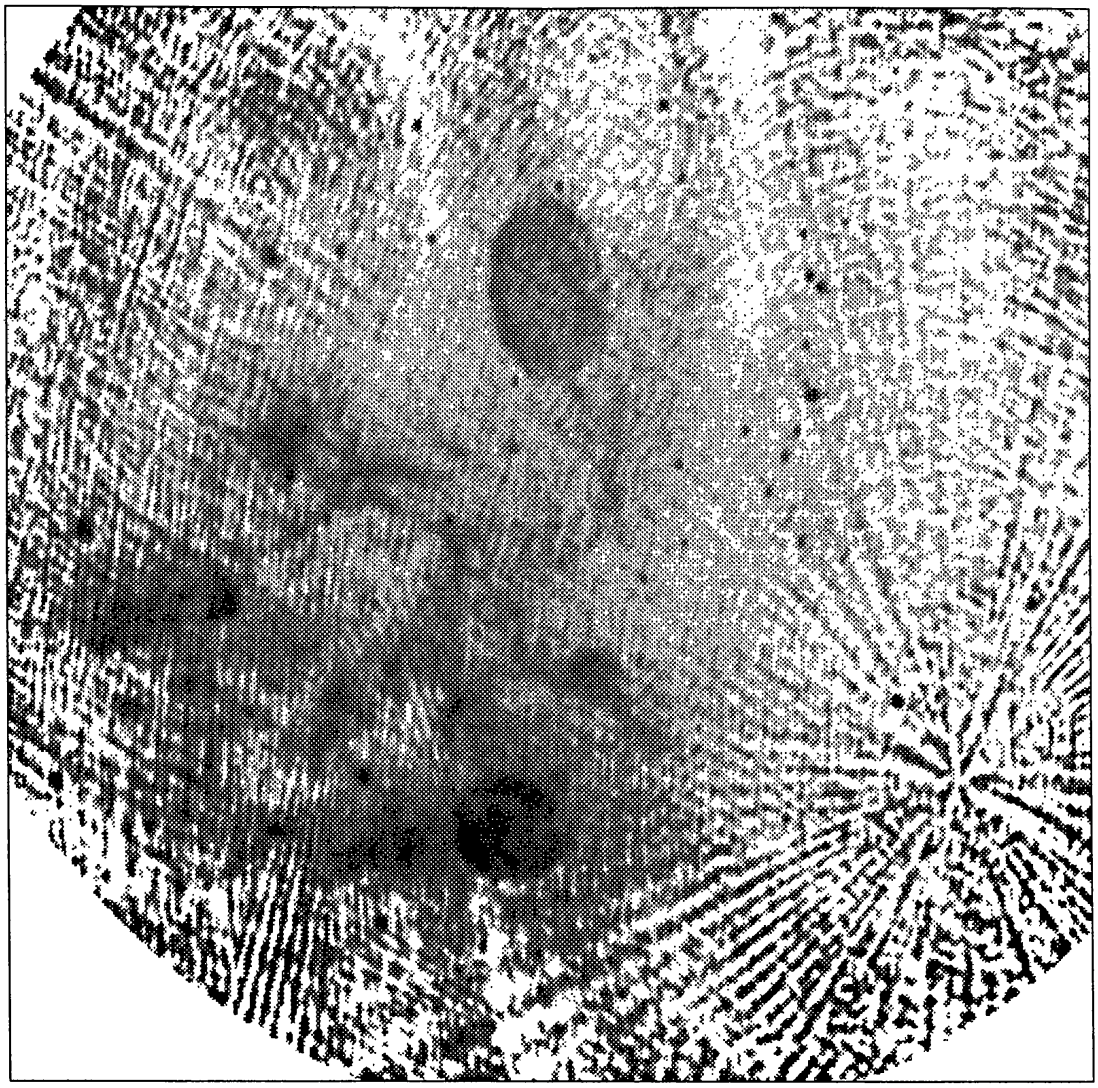

FIG. 1—Grey-scale representation of the 408-MHz field. The observational field centre is slightly to right and above centre. The image has been truncated at a radius of 378′ from the field centre (where the assumed 318′ Gaussian primary pattern has fallen to the 2% level). The low-level features are dominated by instrumental (and possibly atmospheric) effects resulting from the non-perfect removal of Cygnus A, at lower right. At top centre, the SNR W 63 can be seen, while the Cygnus X region of emission fills the lower left quadrant, dominated by the bright SNR G78.2+2.1 (the "γ-Cygni SNR").

figure 1 the field is shown out to a level of 2%. Hence the *rms* noise at the edge of the field in the figure reaches a level of 5.5 Jy/beam!

Results. The map contains a variety of radio sources, with the Cygnus X complex of diffuse emission regions dominating the lower-left portion of the field of view. At top centre is the large, low-surface-brightness supernova remnant (SNR), W63, and at bottom centre is the much brighter SNR, G78.2+2.1, sometimes known as the "γ-Cygni SNR". At the centre of the field, which is slightly to the right and

above the centre of the figure, the radio emission region corresponding to Simeis 57 can be seen. Despite the flaws in the map which result primarily from the presence of Cygnus A, the results presented here represent the best image of the metre-wavelength radio emission from this region that has yet been obtained.

The 408-MHz emission is shown in a set of contour maps presented in figure 2. The radio emission is fully contoured only out to the distance from the field centre where the primary-pattern has dropped to 18%; beyond that, only the highest peaks of emission are plotted. In the inner portion of the field (where the primary-pattern response exceeds 43%), the contour interval is halved to provide more detail. A number of compact radio sources can be seen and these have been analysed by fitting two-dimensional Gaussians to the map data. A list of the sources and derived parameters is presented in Table II. This list should be complete, at least over the area of the field of view where the primary-pattern response exceeds 20%, for flux densities above 1 Jy, but a few weaker sources have also been included. The sources in this list have been numbered as 40P nn, following the Penticton numbering designation (Higgs 1986). The integrated flux density is listed for each source, and for clearly extended sources, an intrinsic source shape is given. For these extended sources, the listed sizes and position angles (counter-clockwise from north) refer to the half-power widths and major-axis orientation of the elliptical Gaussian which, when convolved by the telescope resolution, best fits the map data. Reliable size estimates sometimes could not be derived for sources for which the peak and integrated flux densities differed significantly, and for these a "resolved" comment has been included. For one source that was most easily fitted by a double Gaussian, perhaps because the source is physically double or because of crowding on the sky, a centroid position is listed, along with the positions and flux densities of the two components. In deriving the errors in position and in flux density (all of which are 1σ), uncertainties of 3% in flux density, $0^{s}.5$ in R.A., and $5''$ in Dec. have been combined quadratically with the statistical fitting errors. In the "Comments" column, cross-references to other source designations are given, and the key to these is presented at the end of the table.

The sources in Table II were subtracted from the 408-MHz map and flux densities for some of the diffuse features were then computed. Base-level subtraction is extremely important for large extended features, so the integrated flux densities are somewhat imprecise. Centroid positions and integrated flux densities for these are listed in Table III. Approximate descriptions of the morphology of these extended sources are included along with the identification of associated H II regions.

Comparison with Other Radio Surveys. An adjacent, partially overlapping, field was observed at 408 MHz (and 1.4 GHz) with the DRAO Synthesis Telescope by Wendker *et al.* (1991) earlier in 1985. The 408-MHz compact sources detected in

that survey are denoted by 18P numbers. Since the AGC corrections differed greatly for that survey and for the present one, it is of interest to compare the flux densities derived in the two cases for the sources in common. For these 13 sources, one finds that the ratio of the 40P flux densities to the 18P values is 0.97 ± 0.08, indicating good consistency. Another check on the absolute flux-density scale is that the deduced flux density for Cygnus A in the present observations is 5040 ± 170 Jy. For comparison, the predicted flux density for Cygnus A from the data of Baars *et al.* (1977) is 5055 Jy. With regard to the extended sources, the flux density found here for the SNR G78.2+2.1, 527 ± 55 Jy, agrees well with the value of 540 ± 40 Jy found by Wendker *et al.* (1991).

It should be noted that it is now known that one of the 408-MHz feeds was not performing properly during these observations, and the primary-pattern correction may have systematic errors across the field of view, amounting to as much as ±10% towards the edge of the field in certain position angles. The details of this error are unknown so no correction has been attempted.

One of the more interesting features to appear from the comparison between this survey and the one by Wendker *et al.* (1991), carried out a month earlier, is the strong source visible just at the lower-left edge of the field in figure 1. This compact source, at $\alpha = 20^{h}41^{m}10\overset{s}{.}5 \pm 0.6^{s}$, $\delta = +40°17'09'' \pm 7''$, has a deduced flux density of 37.8±1.5 Jy, and an apparent intrinsic size of $3\overset{'}{.}9 \times 1\overset{'}{.}8$ at a position angle of 48°. No trace of it is seen in the survey by Wendker *et al.* (1991), and it was initially thought to be an example of a radio "flare". It is now considered to be an artefact, as will be described in another paper (Higgs *et al.* 1990).

There now exist several surveys of the Galactic plane with good resolution at other frequencies for comparison with the present data. One can use the recent 1408-MHz observations of Reich *et al.* (1990), the 2695-MHz observations of Fürst *et al.* (1990), and the 4850-MHz survey by Gregory and Condon (1990) to derive spectral indices for many of the sources. These are listed in Table IV. (In this paper, spectral indices, α, will be defined such that the flux density, S, is related to the frequency, ν, by $S \propto \nu^{-\alpha}$). The spectra of some of the candidates for thermal Galactic sources would probably be better fitted with a non-linear spectrum and these are indicated in the Table.

Comparison with Infrared Observations. The IRAS Point Source Catalog (1988) and the IRAS Small Scale Structure Catalog (1988) were searched for sources coincident in position with the radio sources in Table II (within 3′ and having a positional discrepancy less than 3σ) and the extended sources in Table III. The results of this search are presented in Table V. In addition to the listed possible IRAS associations, the infrared sources X 2019+450 (= 20195+4504) and X 2020+448 (= 20204+4450) lie close to the bright south-eastern rim of the SNR W 63 and may be related to it; and X 2021+406 (=20217+4035) lies in the north-eastern rim of the SNR G78.2+2.1, and may be associated with it.

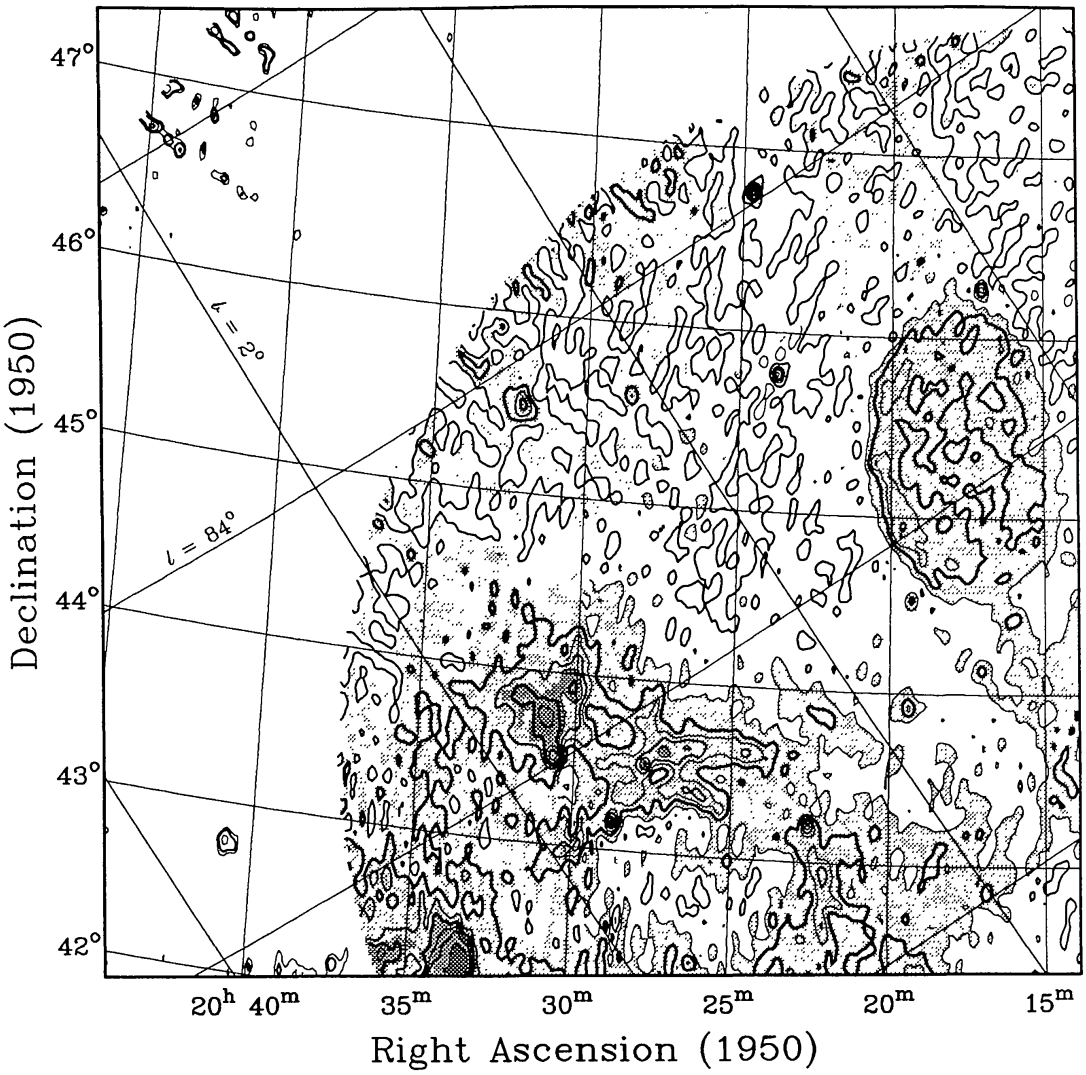

FIG. 2—The distribution of 408-MHz brightness temperature across the field of view, in four overlapping quadrants (a–d). The contour levels, out to a radius of 175′ from the field centre, are 40 K, 80 K, 120 K, 160 K, 200 K, 240 K, 280 K, 320 K, 400 K, 480 K, 640 K, 800 K, 1100 K, 1500 K, and 2000 K. Every second level is drawn with a heavier contour, while the 160-K, 320-K and 1500-K contours are drawn very heavy. In order to minimize confusion near the edge of the field of view where the noise level is high, from a radius of 175′ to 250′, only every second contour (with the heavier pen) is plotted up to a level of 320 K. Four levels of shading are provided to assist the interpretation: <120 K (white); 120 K to 280 K (light); 280 K to 640 K (medium); >640 K (dark). For the outer fringe of the field of view (250′ radius to 378′ radius), only the contours above 320 K are shown. The resolution is 3.4′ × 5.0′ (EW × NS), and 120 K = 1 Jy/beam. The *rms* noise at the centre of the field is estimated to be 110 mJy/beam. A 2° Galactic-coordinate grid is superimposed on the figure.

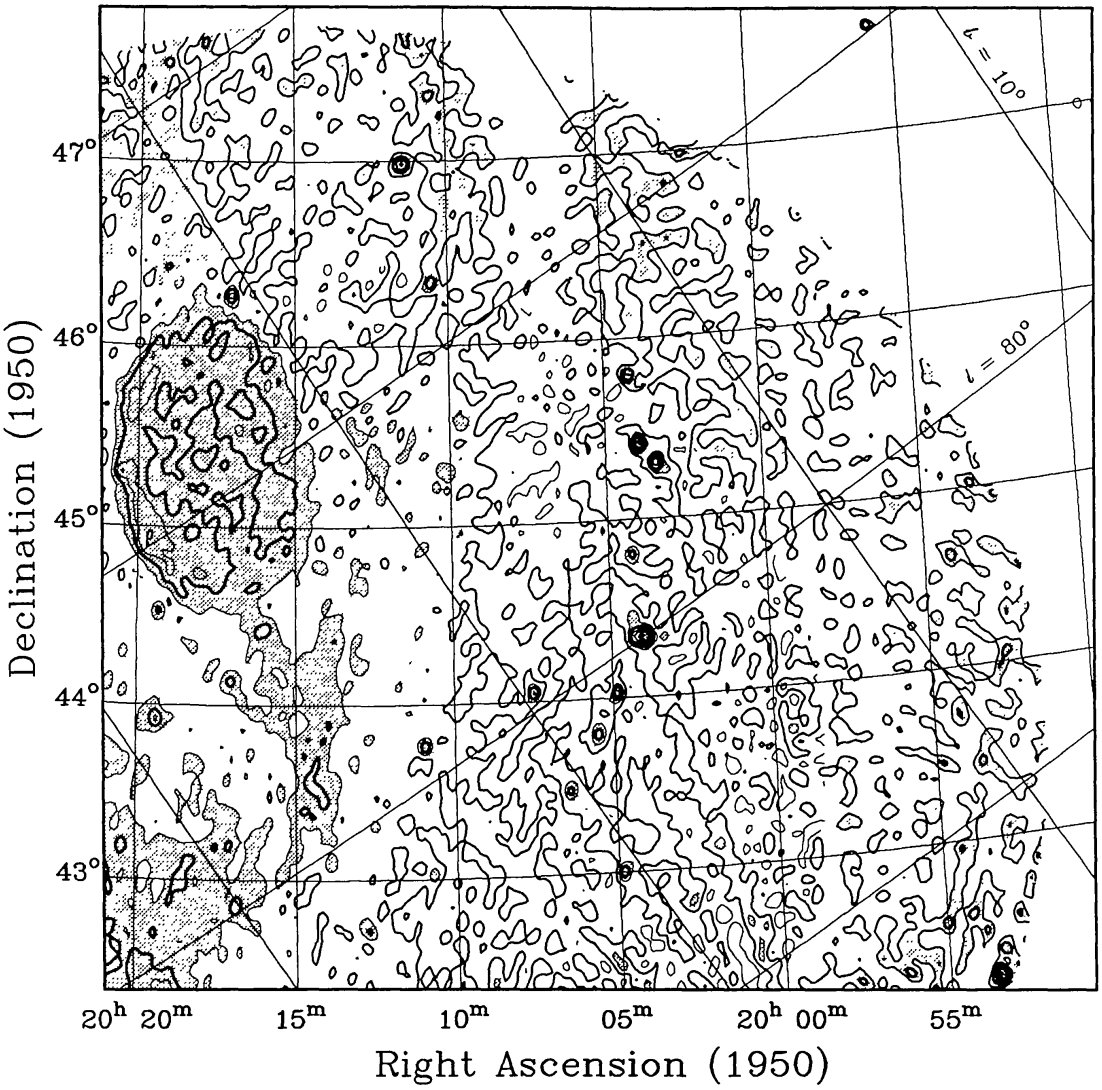

FIG. 2 (*continued*)

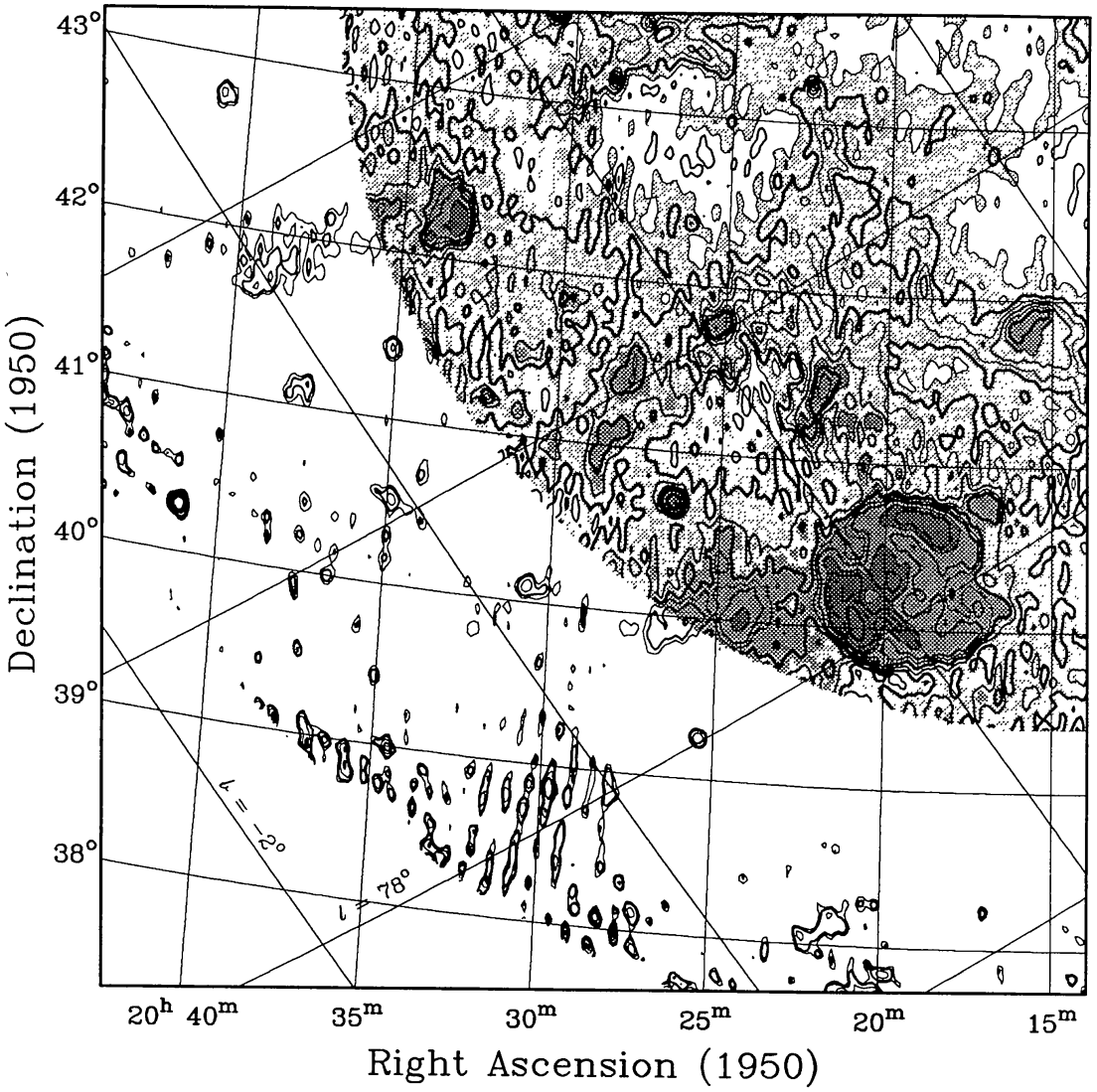

FIG. 2 (*continued*)

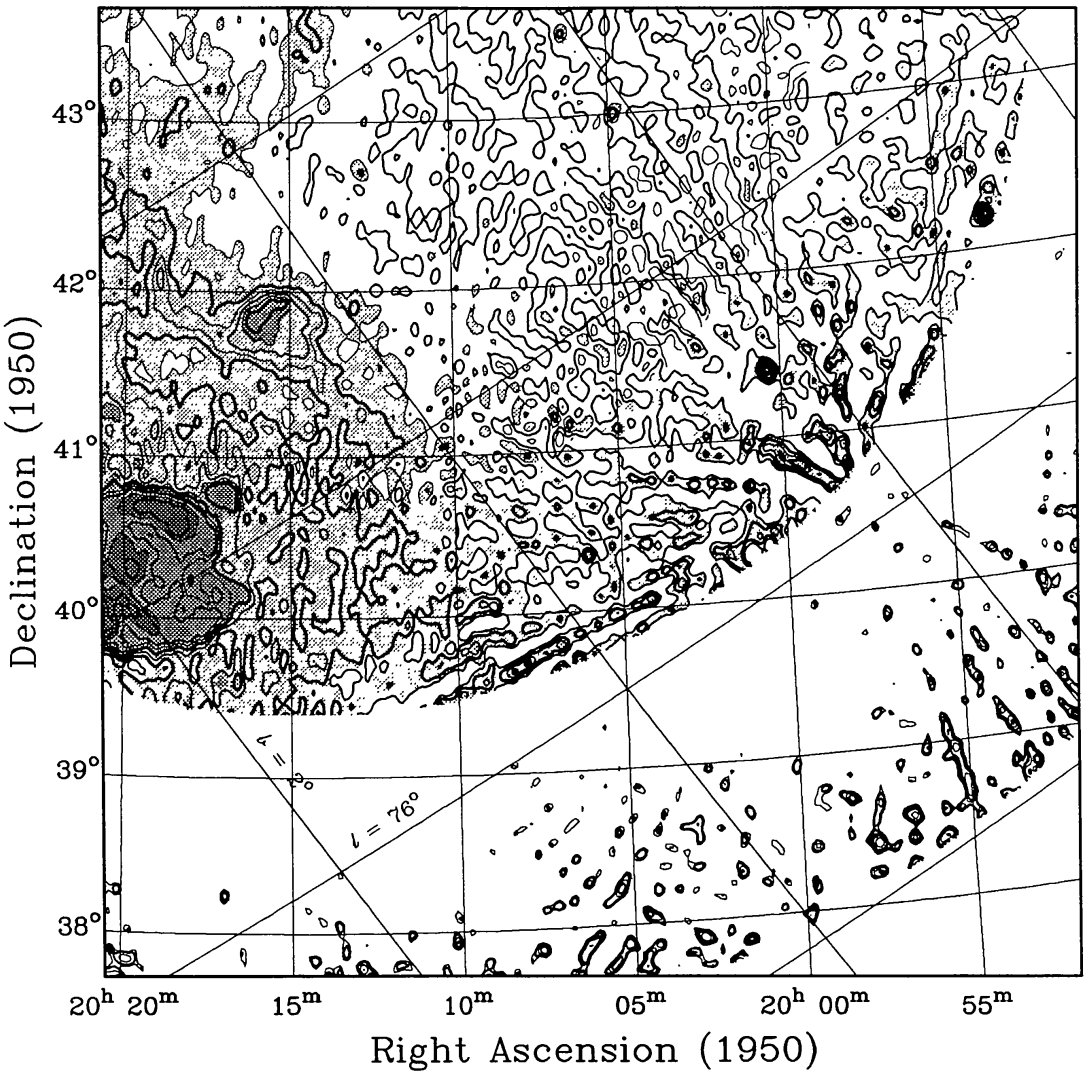

FIG. 2 (*concluded*)

1991JRASC..85...24H

TABLE II
408-MHz Compact Sources

Number (40P)	(1950.0) Right Ascension h m s s	Declination ° ′ ″ ″	Integrated Flux Density mJy	Size ′ × ′	Position Angle °	Comments
1	19 53 30.3 ± 1.4	+42 11 48 ± 15	6100 ± 1700	3.0 × 1.9	97	87GB 1953+4211
2	20 00 24.0 ± 0.5	41 24 23 ± 6	9320 ± 660			
3	20 03 22.5 ± 0.7	45 18 35 ± 9	2350 ± 250	3.2 × 1.4	57	4C +45.42, 87GB 2003+4518
4	20 03 55.8 ± 0.6	45 25 13 ± 7	2250 ± 370			87GB 2003+4524, Galactic?
5	20 04 00.3	44 20 50				centroid
5A	20 03 57.3 ± 0.7	44 20 25 ± 6	4060 ± 250	3.7 × 0.9	97	4C +44.36?, 87GB 2003+4420
5B	20 04 19.5 ± 0.9	44 23 24 ± 37	1360 ± 330			resolved
6	20 04 13.1 ± 0.6	45 47 48 ± 7	1580 ± 210			87GB 2004+4547
7	20 04 15.1 ± 0.8	44 48 08 ± 9	1590 ± 340	3.9 × 2.8	18	87GB 2004+4448
8	20 04 51.0 ± 0.6	43 00 07 ± 8	1070 ± 140			87GB 2004+4300
9	20 04 53.2 ± 0.6	44 01 34 ± 8	1290 ± 170			87GB 2004+4401
10	20 05 30.0 ± 0.6	43 47 47 ± 8	1650 ± 110	4.9 × 2.0	158	87GB 2005+4347
11	20 06 01.0 ± 0.8	40 20 41 ± 12	1780 ± 330			18P 1, F3R 2588, 87GB 2006+4021, optically-thick thermal?
12	20 06 26.1 ± 0.6	43 28 57 ± 7	925 ± 65			87GB 2006+4329
13	20 07 30.1 ± 0.6	44 03 01 ± 6	1400 ± 95			87GB 2007+4403
14	20 10 34.5 ± 0.6	46 20 21 ± 7	1510 ± 105			resolved, 87GB 2010+4619, Galactic?

1991JRASC..85...24H

TABLE II (*continued*)

Number (40P)	(1950.0) Right Ascension h m s s	Declination ° ′ ″ ″	Integrated Flux Density mJy	Size ′ × ′	Position Angle °	Comments
15	20 10 42.0 ± 0.7	43 01 38 ± 9	950 ± 95	3.8 × 1.3	147	87GB 2010+4301
16	20 10 57.4 ± 0.7	43 45 46 ± 8	980 ± 135			4C +43.50
17	20 11 28.9 ± 0.6	46 58 49 ± 6	3320 ± 180			resolved, 4C +46.39, 87GB 2011+4659
18	20 12 46.5 ± 1.1	42 42 23 ± 14	1180 ± 140	5.7 × 0.5	41	18P 5
19	20 12 58.0 ± 1.0	44 13 35 ± 11	450 ± 110			87GB 2012+4413
20	20 13 01.6 ± 1.2	41 54 13 ± 20	660 ± 200			18P 7, 87GB 2013+4153
21	20 14 15.2 ± 0.7	44 46 51 ± 7	815 ± 70	3.4 × 0.3	61	
22	20 16 54.0 ± 0.6	42 50 45 ± 9	1030 ± 85	4.5 × 0.7	161	18P 16
23	20 17 02.8 ± 0.8	46 16 37 ± 10	1010 ± 180			4C +46.40, 87GB 2017+4616
24	20 17 03.4 ± 0.6	44 08 22 ± 11	1030 ± 190	3.4 × 2.0	140	
25	20 19 19.1 ± 0.7	44 32 02 ± 10	1200 ± 130	2.8 × 1.6	0	
26	20 19 23.1 ± 0.6	43 55 14 ± 8	915 ± 70	2.6 × 1.2	18	18P 18, F3R 2698, thermal knot associated with DWB 131?
27	20 20 33.0 ± 0.8	45 18 06 ± 9	690 ± 165			
28	20 22 32.6 ± 0.6	43 13 04 ± 7	1380 ± 125			18P 28
29	20 23 46.3 ± 0.6	45 46 17 ± 7	1750 ± 150			F3R 2731, 87GB 2023+4545
30	20 24 42.1 ± 0.6	46 45 51 ± 7	4430 ± 270	3.9 × 0.9	150	4C +46.41, BG 2024+46?, 87GB 2024+4645

1991JRASC..85...24H

TABLE II (*concluded*)

Number (40P)	(1950.0) Right Ascension h m s s	Declination ° ′ ″ ″	Integrated Flux Density mJy	Size ′ × ′	Position Angle °	Comments
31	20 26 07.0 ± 0.9	42 21 44 ± 11	915 ± 160			18P 41
32	20 26 23.5 ± 0.5	40 41 48 ± 5	13800 ± 500	3.9 × 2.7	75	18P 42, RRF 729, F3R 2653, 87GB 2026+4041, optically-thick thermal
33	20 27 45.2 ± 0.8	43 30 32 ± 10	2360 ± 380	5.1 × 2.6	152	18P 47
34	20 28 32.4 ± 1.1	45 35 20 ± 8	2360 ± 390	4.0 × 2.2	14	BG 2028+45, RRF 752, F3R 2742, 87GB 2028+4535
35	20 28 43.2 ± 0.6	43 09 51 ± 7	1900 ± 145			resolved?, 18P 53
36	20 30 38.6 ± 0.6	43 31 14 ± 7	4590 ± 450	3.3 × 2.6	24	18P 58, in DR 16, part of BG 2030+43?, F3R 2711, 87GB 2030+4330, thermal
37	20 32 08.6 ± 0.7	41 12 45 ± 8	2770 ± 215			resolved?, 18P 61, part of RRF 737, F3R 2682, 87GB 2032+4112, thermal
38	20 34 11.1 ± 0.9	42 07 05 ± 11	3600 ± 500			18P 69

Designations:
4C = Gower *et al.* (1967)
18P = Wendker *et al.* (1990)
87GB = Gregory and Condon (1991)
BG = Fanti *et al.* (1974)
DWB = Dickel *et al.* (1969)
F3R = Fürst *et al.* (1990)
RRF = Reich *et al.* (1990)

1991JRASC..85...24H

TABLE III

SELECTED EXTENDED 408-MHZ SOURCES

Name(s)	(1950.0) R.A. h m s	(1950.0) Dec. ° ′	Shape and Size	Integrated Flux Density Jy	Associated H II Regions
G80.38+4.76	20 14 25	+43 34	faint "bow-tie", 36′(NS) × 12′(EW)	8.2 ± 1.4	Si 57, DWB 111, 118, 119
G79.02+3.62	20 15 25	41 48	30′ patch, brighter in NE	42.0 ± 6.8	IC 1318a, DWB 82, 83
G78.32+2.80 (RRF 722, F3R 2638?)	20 16 55	40 46	irregular 13′ patch	5.8 ± 1.4	DWB 65, 68
G82.16+5.32 (W 63 SNR)	20 17 25	45 21	oval, 100′(NS) × 64′(EW)	165 ± 21	
G78.16+2.12 (γ-Cygni SNR)	20 19 25	40 15	bright 60′ circular patch	527 ± 55	
G82.32+2.42 (DR 16, CXR 10, BG 2030+43?)	20 31 10	43 48	irregular 34′ patch	52 ± 10	DWB 150, 155, 157
G83.78+3.30 (RRF 754, F3R 2748, BG 2032+45)	20 32 05	45 30	isolated 9′ patch	6.9 ± 0.9	DWB 174
G81.36+1.14 (DR 17, BG 2033+42)	20 33 35	42 16	bright 20′ patch	48.0 ± 5.1	

Designations:

BG = Fanti *et al.* (1974)
CXR = Wendker *et al.* (1991)
DR = Downes and Rinehart (1966)
DWB = Dickel *et al.* (1969)
F3R = Fürst *et al.* (1990)
IC = Dreyer (1895)
RRF = Reich *et al.* (1990)
Si = Gaze and Shajn (1955)
W = Westerhout (1958)

TABLE IV
DERIVED SPECTRAL INDICES

Radio Source	Spectral Index	Surveys Used	Comments
40P 1	1.08 ± 0.13	40P, 87GB	
40P 3	1.13 ± 0.07	40P, 87GB	
40P 4	0.53 ± 0.08	40P, 87GB	Galactic?
40P 5A	1.02 ± 0.05	40P, 87GB	
40P 6	0.83 ± 0.07	40P, 87GB	
40P 7	0.98 ± 0.10	40P, 87GB	
40P 8	0.86 ± 0.07	40P, 87GB	
40P 9	1.19 ± 0.08	40P, 87GB	
40P 10	0.94 ± 0.06	40P, 87GB	
40P 11	−0.32 ± 0.15	40P, F3R, 87GB	optically-thin thermal above 2 GHz?, optically-thick at 408 MHz?
40P 12	0.88 ± 0.06	40P, 87GB	
40P 13	0.88 ± 0.06	40P, 87GB	
40P 14	0.60 ± 0.05	40P, 87GB	408-MHz radio source is resolved, Galactic?
40P 15	1.21 ± 0.08	40P, 87GB	
40P 17	0.98 ± 0.06	40P, 87GB†	
40P 19	1.15 ± 0.13	40P, 87GB	
40P 20	1.16 ± 0.15	40P, 87GB	
40P 23	0.96 ± 0.09	40P, 87GB	
40P 26	0.18 ± 0.17	40P, F3R	thermal knot in H II region?
40P 29	1.54 ± 0.11	40P, F3R, 87GB	
40P 30	1.26 ± 0.05	40P, 87GB	
40P 32	−0.05 ± 0.07	40P, RRF, F3R, 87GB†	optically-thick thermal below 1 GHz?
40P 34	1.09 ± 0.08	40P, RRF, F3R, 87GB	
40P 36	0.28 ± 0.26	40P, F3R, 87GB†	optically-thin thermal
40P 37	−0.15 ± 0.09	40P, F3R, 87GB†	optically-thin (?) thermal
G78.32+2.80	−0.28 ± 0.12	40P, RRF, F3R	optically-thick thermal below 3 GHz?
G83.78+3.30	−0.04 ± 0.07	40P, RRF, F3R	optically-thin thermal?

Designations:
† = using estimated integrated flux density
40P = this survey
87GB = Gregory and Condon (1990)
F3R = Fürst *et al.* (1990)
RRF = Reich *et al.* (1990)

TABLE V

RADIO SOURCES COINCIDENT WITH IRAS SOURCES

Radio Source	IRAS Source	Comments
40P 5B	20041+4423	
40P 7	20041+4448	poor positional agreement but radio source is extended
40P 18	20129+4242	poor positional agreement but radio source is extended
G80.38+4.76	20145+4333	Si 57, DWB 118, [MRSL 080+04/5]
G79.02+3.62	X 2015+417	IC 1318a, DWB 82, [MRSL 078+03/1]
40P 25	20193+4430	poor positional agreement but radio source is extended
40P 26	20193+4356	poor positional agreement but radio source is extended, associated with DWB 131?, [MRSL 081+04/2]
40P 32	20264+4042	[RAFGL 2586]
40P 36	X 2030+435	"head" of DR 16
40P 37	20321+4112	[R 57]

Designations (IRAS associations are in [ ]):
DR = Downes and Rinehart (1966)
DWB = Dickel *et al.* (1969)
IC = Dreyer (1895)
MRSL = Marsalkova (1974)
R = 3.24-GHz radio source, reference obscure
RAFGL = Price and Murdoch (1983)
Si = Gaze and Shajn (1955)
X = IRAS Small Scale Structure Catalog (1988)

Discussion of Individual Sources.

a) Non-thermal Galactic Sources. Other than the two known SNRs in the region, only two candidates for Galactic non-thermal sources have resulted from this survey. The sources 40P 4 and 40P 14 have spectral indices around 0.5 and are candidates for further observations. The latter appears extended at 408 MHz but there is no evidence that 40P 4 is extended. Both may well be extragalactic sources with low spectral indices.

The present observations do, however, give the best definition attained to date of the morphology of the W 63 supernova remnant. A detailed discussion of this object will be the subject of another paper, but it is of interest to compare the flux density derived in the present work with earlier determinations. Collected in Table VI are the flux densities found by other investigators. These represent a rather inconsistent data set, mixing high- and low-resolution observations, different techniques for determining baselines and different methodologies for separating the radio emission of H II filaments from that of the SNR. No "critical" evaluation of the data will be made here, and fitting a power-law radio spectrum to the listed values gives the spectrum shown in figure 3. The spectral index is found to be $\alpha = 0.62 \pm 0.07$ if the data points are weighted using the quoted errors, and is $\alpha = 0.49$

TABLE VI
FLUX DENSITIES DERIVED FOR W 63

Frequency (MHz)	Flux Density (Jy)	Reference
178	230 ± 46	Bennett (1963)
408	165 ± 21	present paper
610.5	206 ± 45	Wendker (1968)
750	152 ± 41	Wendker (1968)
960	170 ± 35	Wilson (1963)
1390	100 ± 20	Westerhout (1958)
1414	136 ± 25	Wendker (1968)
1420	170 ± 17	Galt and Kennedy (1968)
2695	112 ± 22	Wendker (1971)
2700	59 ± 3.5	Velusamy and Kundu (1974)
3200	70 ± 21	Higgs *et al.* (1964)
5000	38.5 ± 4.0	Angerhofer *et al.* (1977)

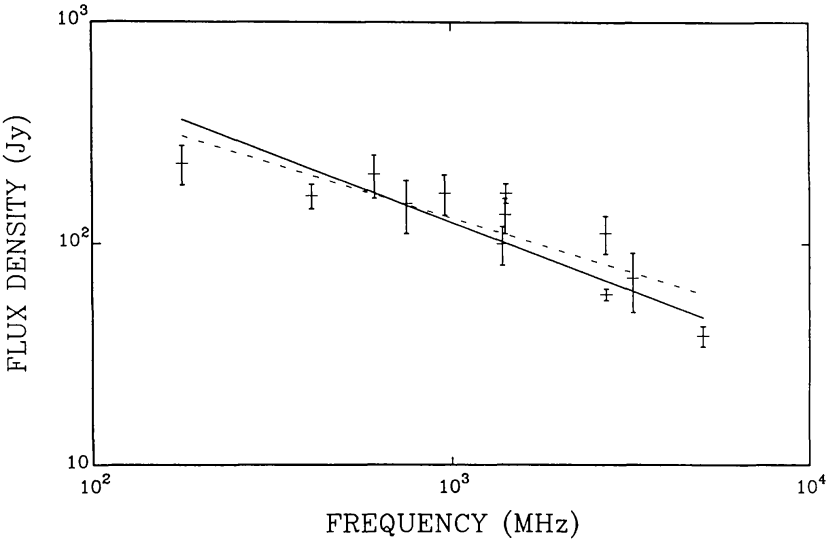

FIG. 3—The radio spectrum of W 63. The solid line gives the best-fitting linear spectrum ($\alpha = 0.62$) when the data points are weighted using their errors, while the dashed line gives an unweighted fit ($\alpha = 0.49$). The flux densities used are listed in Table VI, and no critical evaluation of their reliability or consistency has been attempted.

± 0.09 if no weighting is done. This can be compared with the early value of 0.25 ± 0.15 estimated by Wendker (1968), and the more recent value of −0.77 given by Angerhofer *et al.* (1977). Green (1988) gives a value of "0.7?" in his catalogue of supernova remnants. This relatively steep spectrum depends critically on the 5-GHz point (which actually was a lower limit), and the data in the figure indicate that the true spectrum may be somewhat flatter, perhaps with α closer to 0.5.

b) Simeis 57. The present 408-MHz observations contribute little to our understanding of this peculiar "S-shaped" H II region. Underlying the central "S"

are north-south filaments which delineate a vertical "bow-tie" structure. These lead upwards towards W 63 and downwards towards the bulk of the Cygnus X region. The flux density listed in Table III refers to the brighter portions of these filaments. If the 1420-MHz map (*cf.* Cornwell 1988) is integrated over the same area as was used to arrive at a 408-MHz flux density, a flux density of 5.7 ± 1.5 Jy is found. This gives a spectral index of 0.29 ± 0.26, indicating that the radio emission is probably thermal in nature but not ruling out a non-thermal component of the emission. The morphology of the source is indicative of some sort of "jet" phenomenon; a more detailed analysis of high-resolution observations will be presented in a forthcoming paper (Israel and Bally, in preparation).

c) Other Compact Thermal Sources. From the spectral indices in Table IV and the IRAS associations in Table V, several of the compact sources appear to be good candidates for small H II regions. These are: 40P 5B, 7, 11, 18, 25, 26, 32, 36, and 37. The present results are consistent with the conclusions of Wendker *et al.* (1991) that 40P 32, 36 and 37 are thermal emitters.

Conclusions. A very high-dynamic-range map, but of relatively low sensitivity, has been made at 408 MHz of the radio emission in an 8° field centred on the peculiar H II region Simeis 57. This has provided the best image to date of the very extended supernova remnant W 63. A catalogue of compact sources stronger than 1 Jy has been compiled and some of the extended radio sources have been discussed. In particular, it is possible that the radio emission from Simeis 57 itself may be non-thermal or may have a non-thermal component. Two candidates for new Galactic non-thermal sources have been identified.

Acknowledgements. The Dominion Radio Astrophysical Observatory is operated as a national facility for radio astronomy by the National Research Council of Canada.

L.A. Higgs and T.L. Landecker,
Dominion Radio Astrophysical Observatory,
Herzberg Institute of Astrophysics,
National Research Council of Canada,
Box 248,
Penticton, British Columbia,
V2A 6K3

F.P. Israel,
Sterrewacht Leiden,
Postbus 9513, 2300 RA Leiden,
The Netherlands

and

J. Bally,
AT&T Bell Laboratories,
HOH L-245,
Holmdel, New Jersey 07733,
U.S.A.

References

Angerhofer, P.E., Becker, R.H., and Kundu, M.R., 1977, *Astron. Astrophys.*, **55**, 11.

Baars, J.W.M., Genzel, R., Pauliny-Toth, I.I.K., and Witzel, A., 1977, *Astron. Astrophys.*, **61**, 99.

Bennett, A.S., 1962, *Mem. Roy. Astron. Soc.*, **68**, 163.

Bennett, A.S., 1963, *Monthly Notices Roy. Astron. Soc.*, **127**, 3.

Clark, B.G., 1980, *Astron. Astrophys.*, **89**, 377.

Cornwell, T.J., 1988, *Astron. Astrophys.*, **202**, 316.

Dickel, H.R., Wendker, H., and Bieritz, J.H., 1969, *Astron. Astrophys.*, **1**, 270.

Downes, D., and Rinehart, R., 1966, *Astrophys. J.*, **144**, 937.

Dreyer, J.L.E., 1895, "*Index Catalogue of Nebulae*" (1953 reprint), *Mem. Roy. Astron. Soc.*, London.

Edge, D.O., Shakeshaft, J.R., McAdam, W.B., Baldwin, J.E., and Archer, S., 1959, *Mem. Roy. Astron. Soc.*, **68**, 37.

Fanti, C., Felli, M., Ficarra, A., Salter, C.J., Tofani, G., and Tomasi, P., 1974, *Astron. Astrophys. Suppl.*, **16**, 43.

Fürst, E., Reich, W., Reich, P., and Reif, K., 1990, *Astron. Astrophys. Suppl.*, **85**, 805.

Galt, J.A., and Kennedy, J.E.D., 1968, *Astron. J.*, **73**, 135.

Gaze, V.F., and Shajn, G.A., 1951, *Izv. Krym. Astrofiz. Obs.*, **7**, 93.

Gaze, V.F., and Shajn, G.A., 1955, *Izv. Krym. Astrofiz. Obs.*, **15**, 11.

Gower, J.F.R., Scott, P.F., and Wills, D., 1967, *Mem. Roy. Astron. Soc.*, **71**, 49.

Green, D.A., 1988, *Astrophys. Space Sci.*, **148**, 3.

Gregory, P.C., and Condon, J.J., 1990, private communication.

Haslam, C.G.T., Salter, C.J., Stoffel, H., and Wilson, W.E., 1982, *Astron. Astrophys. Suppl.*, **47**, 1.

Higgs, L.A., 1986, *J. Roy. Astron. Soc. Canada*, **80**, 51.

Higgs, L.A., Broten, N.W., Medd, W.J., and Raghavarao, R., 1964, *Monthly Notices Roy. Astron. Soc.*, **127**, 367.

Higgs, L.A., Landecker, T.L., and Wendker, H.J., 1990, in preparation.

IRAS Point Source Catalog, 1988, *Infrared Astronomical Satellite (IRAS): Catalogs and Atlases*, **2**, NASA Ref. Publ. 1190, U.S. Government Printing Office.

IRAS Small Scale Structure Catalog, 1988, *Infrared Astronomical Satellite (IRAS): Catalogs and Atlases*, **7**, NASA Ref. Publ. 1190, U.S. Government Printing Office.

Joncas, G., and Higgs, L.A., 1990, *Astron. Astrophys. Suppl.*, **82**, 113.

Marsalkova, P., 1974, *Astrophys. Sp. Sci.*, **27**, 3.

Reich, W., Reich, P., and Fürst, E., 1990, *Astron. Astrophys. Suppl.*, **83**, 539.

Roger, R.S., Costain, C.H., Lacey, J.D., Landecker, T.L., and Bowers, F.K., 1973, *Proc. I.E.E.E.*, **61**, 1270.

Steer, D.G., Dewdney, P.E., and Ito, M.R., 1984, *Astron. Astrophys.*, **137**, 159.

Veidt, B.G., Landecker, T.L., Vaneldik, J.F., Dewdney, P.E., and Routledge, D., 1985, *Radio Science*, **20**, 1118.

Velusamy, T., and Kundu, M.R., 1974, *Astron. Astrophys.*, **32**, 375.

Wendker, H., 1968, *Z. Astrophys.*, **69**, 392.

Wendker, H.J., 1971, *Astron. Astrophys.*, **13**, 65.

Wendker, H.J., Higgs, L.A., and Landecker, T.L., 1991, *Astron. Astrophys.*, in press.

Westerhout, G., 1958, *Bull. Astron. Inst. Netherlands*, **14**, 215.

Wilson, R.W., 1963, *Astron. J.*, **68**, 181.